High-resolution 3D structural and optical analyses of hybrid or composite materials by means of scanning probe microscopy combined with the ultramicrotome technique: an example of application to engineering of liquid crystals doped with fluorescent quantum dots

Konstantin E. Mochalov[a,b], Anton E. Efimov[c,d], Alexey Yu. Bobrovsky[e], Igor I. Agapov[c], Anton A. Chistyakov[a], Vladimir A. Oleinikov[a,b], Igor Nabiev[a,f,*]

[a] Laboratory of Nano-Bioengineering, Moscow Engineering Physics Institute, 115409 Moscow, Russian Federation; [b] Shemyakin–Ovchinnikov Institute of Bioorganic Chemistry, Russian Academy of Sciences, 117997 Moscow, Russian Federation; [c] Laboratory of Bionanotechnology, Shumakov Federal Research Center of Transplantology and Artificial Organs, 123182, Moscow, Russian Federation; [d] SNOTRA LLC., 105318, Moscow, Russian Federation; [e] Faculty of Chemistry, Moscow State University, 119991 Moscow, Russian Federation; [f] Laboratory of Research in Nanosciences, EA4682, Université de Reims Champagne-Ardenne, 51100 Reims, France

ABSTRACT

Combination of nanometer-scale 3D structural analysis with optical characterization of the same material is a challenging task. Its results may be important for nanophotonics, materials science, and quality control. We have developed a new technique for complementary high-resolution structural and optical characterization followed by optical spectroscopic and microscopic measurements accompanied by reconstruction of the 3D structure in the same area of the sample. The 3D structure is reconstructed by combination of ultramicrotomic and SPM techniques allowing the study of the 3D distribution of implanted nanoparticles and their effect on the matrix structure. The combination of scanning probe nanotomography (SPN) and optical microspectroscopy makes it possible to direct estimate how the 3D structural characteristics of materials affect their macroscopic optical properties. The technique developed has been applied to the engineering of materials made from cholesteric liquid crystals and fluorescent quantum dots (QDs). These materials permit photochemical patterning and image recording through the changes in the dissymmetry factor of circular polarization of QD emission. The differences in the polarisation images and morphological characteristics of the liquid crystal matrix have proved to be correlated with the arrangement of the areas of homogeneous distribution and non-homogeneous clustering of QDs. The reconstruction of the 3D structure of the liquid crystal matrix in the areas of homogeneous QD distribution has shown that QDs embedded into cholesteric liquid crystal matrices do not perturb their periodic planar texture. The combined optical/SPM/ultramicrotome technique will be indispensable for evaluating the effects of inorganic nanoparticles on the organisation of organic and liquid crystal matrices, biomedical materials, cells, and tissues.

Keywords: Scanning probe microscopy, 3D structural analysis, optical microspectroscopy, liquid crystals matrix, fluorescent quantum dots

1. INTRODUCTION

In materials science, the request for local information at the nanometer scale makes high-resolution microscopy techniques essential tools for morphology characterization. In this respect, transmission and scanning electron microscopies (TEM, SEM) and scanning probe microscopy (SPM) are the most important techniques extensively used for characterization of nanomaterials and nanocomposites. Standard high-resolution microscopy mainly provides

* igor.nabiev@gmail.com; phone: +33-631 259 180

Integrated Photonics: Materials, Devices, and Applications II, edited by Jean-Marc Fédéli, Laurent Vivien, Meint K. Smit, Proc. of SPIE Vol. 8767, 876708 · © 2013 SPIE · CCC code: 0277-786X/13/$18 · doi: 10.1117/12.2017088

information on either the lateral organization of the specimen (two-dimensional (2D) projection images of thin-film specimens obtained by TEM) or the topography of the specimen surface (SEM and SPM). In modern functional materials research, however, information on the 3D local nanoscale spatial organization of complex material systems becomes more and more important. In fact, better understanding of essential parameters determining interface organization in the bulk of materials systems, phase separation and network formation in polymer blends and composites, distribution of aggregations of nanoscale dopants and nanoparticles, and its influence on the macroscopic properties of materials makes nanoscale spatial information crucial.[1] This is the reason why three-dimensional (3D) or tomographic imaging of the organization of complex material systems is one of the most intensely developing areas of modern microscopy.

Recently, advances in instrument and software development made electron tomography (ET), also referred to as 3D TEM, a versatile tool for nanoscale 3D reconstruction of biological and polymer materials.[2] A series of 2D TEM projection images of thin sections of a sample are obtained at different angles, for which purpose the specimen is tilted relative to the electron beam. After off-line alignment and reconstruction, a 3D image of the specimen is obtained.[1-5] However, the thickness of the analyzed section is limited to 100–300 nm, which is therefore the maximal depth of 3D analysis. An alternative approach to volume reconstruction is the so-called "slice-and-view," in which the 3D morphology is obtained by repetitively cutting away some material from the sample by the focused ion beam (FIB) technique and subsequently imaging the fresh surface by means of SEM.[6,7] In this case, however, the problem is that polymers and biological materials are very electron- and ion-beam-sensitive, and their initial organization may be altered if the electron dose exceeds a low critical value.[8,9]

In contrast to electron microscopy, SPM can be regarded as a nondestructive surface characterization technique for soft matter analysis,[10,11] which may overcome some of the aforementioned limitations of EM because it does not induce any radiation damage of the sample surface. A promising recent approach to 3D nanotomography is based on combining SPM with an ultramicrotome.[12-15] In this case, SPM measurements can be performed immediately after microtoming at the fresh surface of an untreated block face.[16,17] The depth resolution is only limited by the thickness of sections removed from the block face surface; it can be as fine as 10 nm. The maximum thickness of the reconstructed sample image is, in principle, unlimited; analysis of specimens as thick as several micrometers is quite practicable.
The development of modern nanohybrid materials with controlled optical properties raises the problem of evaluation of the correlation between their optical properties and 3D morphological structure. This requires a new experimental technique for complementary optical and 3D morphological analyses of nanohybrid systems. The main demands for such a technique should be the possibility of high-resolution microscopy (EM, SPM) and different types of optical microspectroscopy in the same area of a nanohybrid sample. Good examples of nanohybrid material are systems of fluorescent quantum dots (QDs) incorporated in liquid crystal matrices.[18] Nanohybrid structures of this type are especially interesting because they effectively combine unique optical properties of nanosized materials with the possibility of arranged distribution of QDs in liquid crystal matrices, which allows for optical and electro-optical control of the properties of these structures.[19-24] The development of QD/LC structures was originally focused on the use of nematic liquid crystal (LC) matrices, which had wide industrial applications and were well studied.[18] Recently, however, a number of researchers have turned to incorporation of fluorescent CdSe/Zns and CdSeTe QDs into cholesteric LC matrices (CLC matrices). These low-molecular-weight polymer-based cholesteric liquid crystals are smart stimulus-responsive materials with promising applications in optoelectronics and photonics.[25] New optical materials based on CLCs doped with fluorescent CdSe/ZnS QDs have been developed and demonstrated to have a wide photonic bandgap.[26-29] It has been shown that the fluorescence emission of QDs embedded in LCs is circularly polarized and that the dissymmetry factor of this polarization may be optically or electrically controlled via conformational changes in the helical structure of the LC matrix.[29] The capability of photochemical patterning or image recording using these materials has been demonstrated; the recorded information can be read on the basis of changes in the dissymmetry factor of circular polarization of QDs emission. The developed photo- and electro-active materials with a controlled degree of fluorescence circular polarization may be used as on-demand single photon sources in photonics, optoelectronics, and quantum cryptography,[30,31] as well as for the development of nanophotonic systems capable of low-threshold lasing.[32]

It is obvious that a high efficiency of optical devices based on QD/CLC systems requires maximizing the concentration of homogeneously dissolved QDs in the CLC matrix. Therefore, the corresponding analytical procedure is necessary to study the local 3D distribution and aggregate state of QDs in the sample (to determine whether individual QDs are distributed homogeneously or aggregated in clusters) and the influence of the QD distribution nanomorphology on the

optical properties of QD/CLC. This technique should provide complementary information about the 3D topology of the QD distribution and cholesteric matrix structure at the nanolevel (TEM, SEM, or AFM) and local optical properties of the system (polarized optical microscopy (POM) and fluorescent microspectroscopy) from the same area of the sample. To date, no complementary analytical technique suitable for this purpose is known. A few recent studies[-35] dealt with 3D-structure analysis of CLC systems (but without any nanosized dopants) with the use of the TEM, SEM, POM, and AFM techniques; however, in none of them were the optical and nanomorphological properties studied in the same site of a sample.

2. RESULTS AND DISCUSSION

Here, we present a new analytical technique that allows complementary AFM, POM, and fluorescent microspectroscopy data to be obtained for the same area of the sample and reconstruct the 3D nanostructure of the sample by means of scanning probe nanotomography (SPN). SPN comprises a new methodology and unique instrumentation for 3D reconstruction of the nanoscale organization and corresponding functional properties of soft matter recently developed by our research group.[12] It combines SPN with an ultramicrotome[14] or cryoultramicrotome.[13] This combination makes it possible to analyze directly a block face surface immediately after each ultramicrotome section is made and can be applied to serial section tomography of a wide range of soft biological and polymer materials in the native state. This is followed by the reconstruction of 3D structures of the objects through integration of surface images for successive ultrathin sections. Note also that, in principle, this technique places no limitation on the thickness of the sample analyzed. The SPN technique has been successfully applied to studying the 3D structures of biological objects and different advanced materials, such as polymer blends, polymer/nanotube[14] and polymer/graphene[15] nanocomposites. However, this methodology has not been combined with correlative light microscopy required for comprehensive analysis of 3D nanostructure morphology and optical properties of nanohybrid optical materials. The step-by-step experimental procedure is schematically shown in Figure 1.

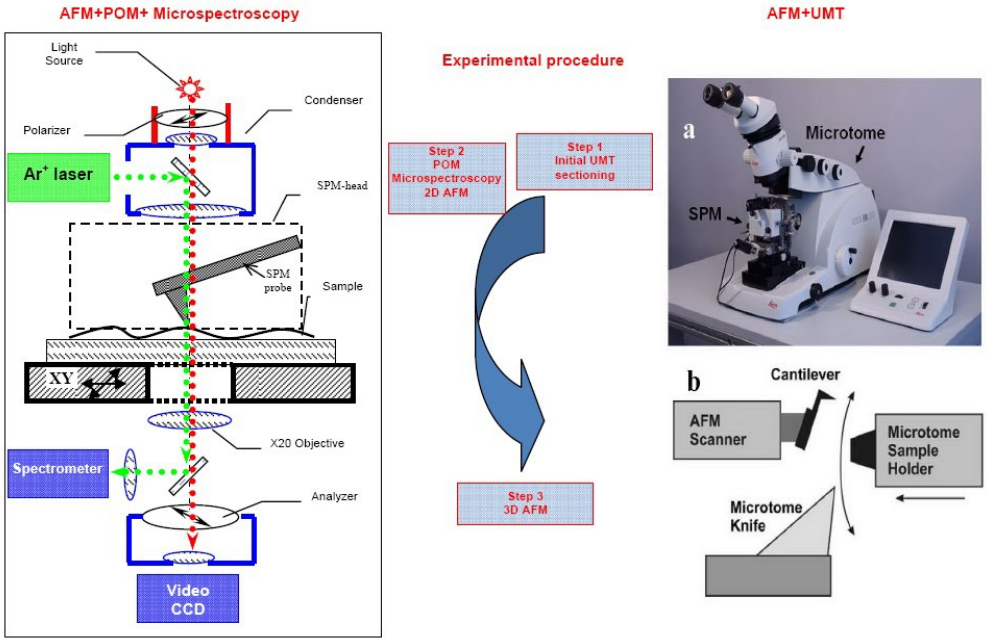

Figure 1. Experimental apparatus and procedure for structure characterization of CLC matrices with embedded fluorescence QDs that allows for AFM, transmission POM, and fluorescence microspectroscopy measurements, as well as for 3D reconstruction of the sample structure by the SPN technique for the same site in the sample.

Left panel: schematic diagram of the combined apparatus for complementary AFM, POM. and confocal microscopy measurements.

Right Panel: (a) overview of AFM/ultramicrotome setup; (b) schematic diagram of the AFM/ultramicrotome system operation. The sequence of the experimental procedures required for all complementary measurements is shown.

The first step consists in initial ultramicrotome sections of the QD/CLC sample deposited on a glass substrate in order to obtain a flat block face surface for AFM/POM/fluorescence correlative microscopy. These sections are made in the plane parallel to the glass substrate and perpendicular to the helix axis. Then, the sample is transferred to a combined AFM/POM/fluorescence device for AFM and POM imaging and spectroscopic measurement of planar and defect sectioned areas of the sample. After that, the sample is transferred back to the AFM/UMT system, where we locate the same surface areas on the block face by means of AFM and optical microscopy and then proceed with ultramicrotome sectioning of controlled uniform thickness and subsequent AFM measurements to obtain nanotomography 3D reconstruction.

A glass-forming cyclosiloxane matrix of the type described in our previous studies[27,28] served as a CLC matrix This matrix was characterized by a selective light reflection peak for left-handed circularly polarized light at $\lambda = 450$ nm, a clearing temperature of 180–182°C, and a glass transition temperature of approximately 50°C. As a chiral photochromic dopant responsible for helix phototuning properties, a derivative of isosorbide and cinnamic acid (Sorb) was used. It is characterized by a high helical twisting power and induces the formation of a right-handed supramolecular helical structure in the cholesteric matrix. UV irradiation induces thermally irreversible E–Z isomerization of Sorb at C=C bonds, which is accompanied by a decrease in the helical twisting power. Therefore, introduction of Sorb as a dopant into a cyclosiloxane CLC matrix leads to partial untwisting of the helix and, hence, a red shift of the selective light reflection peak. Subsequent UV irradiation results in a reverse shift of the selective light reflection peak to shorter wavelengths.

We used CdSe and ZnS semiconductor QDs with emission wavelengths of 530 and 604 nm, respectively, as fluorescent dopants. After incorporation of a small amount of QDs of these types, the clearing temperature shifts to 170–172°C, which is 10°C lower than that of a pure cyclosiloxane CLC matrix, whereas the glass transition temperature is the same (~50°C).

Initial analysis of this structure by means of POM did not show any signs of aggregation and phase separation in most of the area of the planar-oriented films; hence, the obtained composite material was sufficiently homogeneous. However, for manufacturing QD/CLC systems with a high concentration of QDs, which is necessary for lasing and other applications, we have to know the true 3D structure of the nanocomposites produced, the maximal achievable concentration of homogeneously distributed QDs in the CLC matrix, and the influence of QD clusters on the optical properties of the QD/CLC hybrid structure. Therefore, we developed and tested the technique for complementary optical–morphological analysis described above.

Figure 2a shows a POM image of an ultramicrotomed area of a QD/CLC sample (step 1 and 2 in Fig. 1). Note that POM is a conventional technique for assessing the quality of CLC structures,[25] because ideal structures of this type should turn transmitted linearly polarized light into elliptically polarized one; hence, they are seen as bright fields in POM images (marked with a green circle in Fig. 2a). This is not the case with defect areas; they are observed as dark stains on POM images (marked with a blue circle in Fig. 2a). The oily streaks observed are typical defects of such LC structures even without any dopants, whereas the defect in the circled area is caused by aggregation of QDs.

We have recorded and analyzed microfluorescence spectra of the left- and right- handed circularly polarized components from areas marked with the green and blue circles (Fig. 2b, the diameter of the exciting laser spot was 40 μm), i.e., the planar and defect areas of the QD/CLC sample. As can be seen in Fig. 2b, the QD aggregates causing defects have a fluorescent spectrum (Defect) that is a superposition of the fluorescence spectra of QDs embedded in the LC matrix (530 and 604 nm). The left-handed circularly polarized component of the fluorescence spectrum of nonaggregated QDs is modified by the peak of selective light reflection (590 nm). This modification, together with the high negative fluorescence dissymmetry factor (Fig. 2c), indicate a regular planar structure of the CLC matrix in this area.

However, the following questions remain unanswered: (1) Are QDs in the planar zone located separately from each other or they aggregate into microclusters? and (2) What are the proportions of QDs homogeneously distributed in the CLC matrix and aggregated in clusters (in other words, what is the QD solubility in the CLC matrix)? To answer these questions, we have used the advantages of the SPN technique. A 2D AFM image (Fig. 3a) corresponding to the area marked with a black square in Fig. 2a is a reference for the 3D reconstruction of the QD distribution in the planar and defect zones of the QD/CLC sample, and the boundary between the two areas is clearly seen. Note that the cutting plane

is perpendicular to the CLC helix axis; in this case, we a much less of characteristic background topography is seen, which considerably complicates the reconstruction of the 3D distribution of individual QDs. Figure 3b shows AFM images of QDs in the planar area (Fig 3a), and here we can clearly see two individual QDs. The cross-section of this AFM image shown in Fig. 3c proves that these are indeed single QDs, because their measured height does not exceed 10 nm, what corresponds to the diameter of a QD with a TOPO shell partly embedded into the CLC matrix.

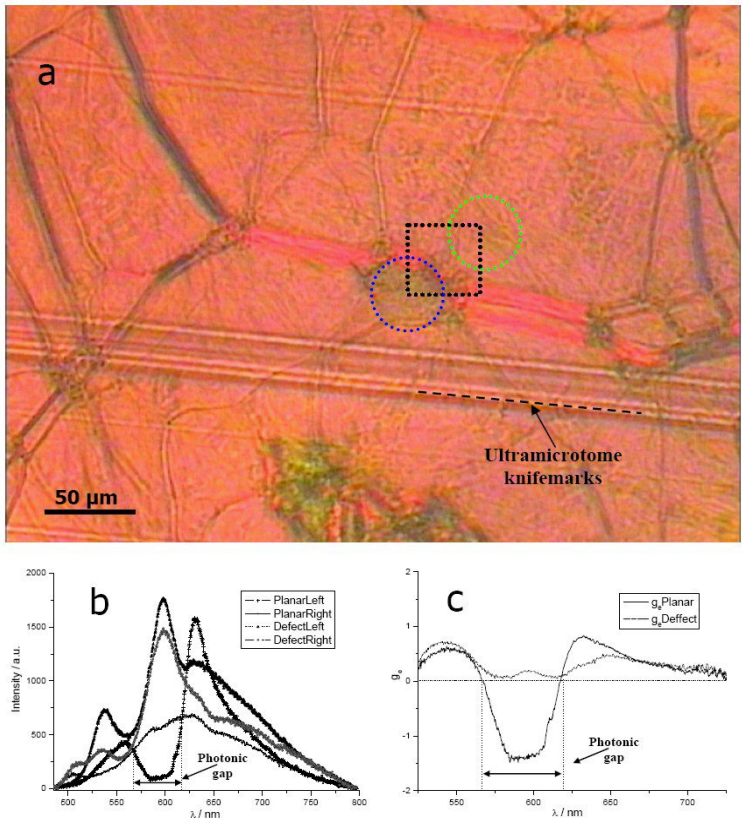

Figure 2. Analysis of the influence of aggregation of QDs embedded in a CLC matrix on their fluorescence characteristics.

(a) A POM image of the ultramicrotomed area of a QD/CLC surface. The green circle marks the area for which "planar zone" fluorescence spectra have been recorded. The blue circle marks the area for "defect zone" fluorescence spectra have been recorded. The black square is the area AFM-scanned (Fig. 3a) containing both planar and defect zones.

(b) The right- and left-handed circularly polarized components of the fluorescence emission spectrum of QDs embedded in the CLC matrix. Considerable modulation of left-handed circularly polarized component of the fluorescence emission spectrum of QDs in the area of the peak of selective light reflection in the LC matrix (λ = 590 nm) is seen in the planar zone. In the defect zone, the modulation is not pronounced.

(c) Fluorescence dissymmetry factors of QDs embedded in the planar and defect zones of the CLC matrix. A high negative fluorescence dissymmetry factor has been found in the planar zone. $g_e = 2(I_L - I_R) / (I_L + I_R)$, where I_L and I_R are, respectively, the left- and right-handed circularly polarized components of the QD fluorescence spectrum.

The use of the SPN technique allows the reconstructions of the QD distribution in the CLC matrix in both planar and defect areas at the same spot as in Fig 3a (Step 3 in Fig. 1). Figures 4a and 4b show the 3D structural analysis of the QD distributions in the planar and defect areas of the CLC matrix. Analysis of SPN data shows that QDs in the defect zone are aggregated in separate mini-clusters with an average diameter of about 1.5 µm. Although these mini-clusters are much smaller than the total thickness of the CLC-matrix, they are large enough to destroy the planar structure in this

zone of the sample. We propose the following routine for the determination of the amount and concentration of homogeneously distributed QDs and the corresponding value of their solubility in the CLC matrix based on the SPN data shown in Fig. 4a.

The mass fraction of homogeneously dissolved particles is given by the equation

$$w_{homo} = (\rho/\rho_0)\cdot N\cdot v_{QD,} \quad (1)$$

where $\rho = 5.8$ g/cm^3 is the density of the CdSe core, which is a fairly accurate approximation of the density of the overall density of the QD; $\rho_0 \approx 1$ g/cm^3 is the density of the CLC matrix; $v_{QD} = 1.715\cdot10^{-25}$ m^3 is the mean volume of a QD without the TOPO shell, whose weight is much less than that of the CdSe core (the density of TOPO is 0.88 g/cm^3); and N is the volume concentration of QDs in the volume studied. N is calculated as

$$N = (N_{obs}/V)\cdot(h/d_{QD}), \quad (2)$$

where N_{obs} is the counted number of QDs in the 3D reconstruction (according to Fig. 4a, $N_{obs} = 22$); h = 50 nm is the thickness of the ultramicrotome section; V = 17.5 um^3 is the analyzed volume (Fig. 4a); and $d_{QD} \approx 10$ nm is the mean diameter of a QD with the TOPO shell. Therefore, we can calculate that volume concentration of homogeneously dissolved QDs in the volume studied: $N = (6.28 \pm 1.33)\cdot10^{18}$ m^{-3}. Thus, according to Equation (1), the homogeneous solubility of QDs in the CLC matrix (w_{homo}) is $(6.25 \pm 1.32)\cdot10^{-4}$ wt%. Given an initial mass fraction of the embedded QDs of 0.25 wt%, we obtain that, in our case, only one out of 40 QDs embedded is dissolved homogeneously in the CLC matrix.

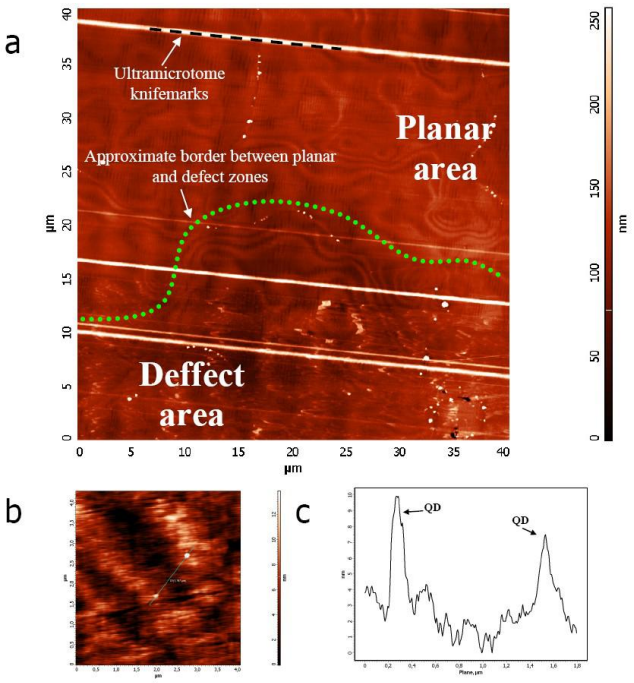

Figure 3. Structural analysis of the 2D and 3D distributions of QDs embedded in the cluster and homogeneous distribution zones of a CLC matrix.

(a) A 2D AFM image of a QD/CLC sample area (40 × 40 μm) including both planar and defect zones.

(b) A 2D AFM image of the planar zone of a QD/CLC system containing single QDs.

(c) Cross-section of the AFM image shown in Fig. 3b across the marked line.

Analysis of the POM images and integrated fluorescence spectra recorded from large areas of these QD/CLC structures (the diameter of the excitation laser spot was 2 mm) proves that the major part of the QD/CLC sample has a planar structure without defects.[27,28] This can be explained by the fact that, although most QDs (more than 97%) are aggregated in clusters, the defect zones themselves are very compact and take up little of the total volume of QD/CLC system. Hence, they do not considerably distort its integrated optical properties. Regarding the engineering of optical devices where the QD fluorescence is modulated by the CLC matrix, we may conclude that the main disadvantage of QD/CLC systems is a very low concentration of homogeneously dissolved QDs, which leads to a low emittance of these structures. At the same time, the defects caused by QD incorporation has almost no effect on the integrated optical properties. Therefore, our results confirm that the development of surfactants highly specific to CLC matrices (similar to those described in recent studies[36-38]) that could be effective substitutes for TOPO on the surface of QDs and, hence, sufficiently increase the homogeneous solubility of QDs, is the most important challenge in the development of optical devices based on fluorescent QDs embedded in CLC matrices.

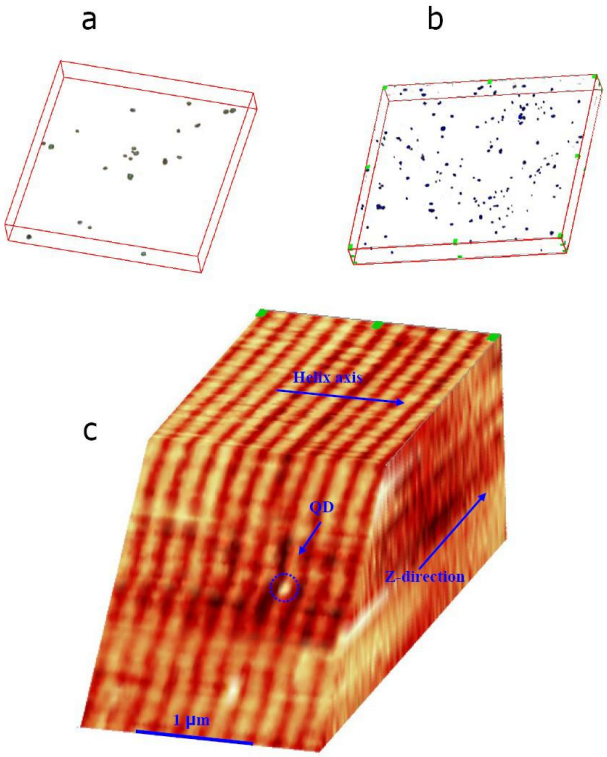

Figure 4. Influence of single QDs within the CLC matrix on its planar structure.

(a) An SPN 3D reconstruction of the QD distribution in the planar zone of the QD/CLC structure. A homogeneous distribution of single QDs is observed. The Z axis corresponds to the cholesteric helix axis of the CLC matrix. The sizes of the reconstructed volume are 5.0 × 5.0 × 0.7 µm.

(b) An SPN 3D reconstruction of the QD cluster distribution in the defect zone of the QD/CLC structure. The Z axis corresponds to the cholesteric helix axis of the CLC matrix. The sizes of the reconstructed volume are 50 × 50 × 5.0 µm.

c) An SPN 3D reconstruction of the periodic structure of the planar zone of the CLC matrix doped with QDs. The Z direction is perpendicular to the cholesteric helix axis of the CLC matrix. The blue circle marks one of the individual QDs embedded in the matrix.

The last but no less important result to be discussed here is the influence of a single QD on the planar structure of the CLC matrix in its vicinity. Although the results described above showed that the overall planar structure was not disturbed in the zones of homogeneous QD distribution, it was still possible that the structure was affected in the near vicinity of each QD but recovered with increasing distance from it. This question is crucial for determination of the

maximum possible concentration of single QDs in the matrix: the smaller the defect zone near a QD, the larger the limit QD concentration in the planar matrix structure. To answer this question, we performed an SPN 3D reconstruction of a QD/CLC sample in the planar zone, with the section plane parallel to the helix axis. This allowed us to clearly observe the characteristic periodic structure on the surface corresponding to the pitch of the cholesteric helix structure. Figure 4c shows the reconstructed 3D SPN image of the QD/CLC structure in the zone of homogeneous QD distribution. There are no aggregations or distortions of the planar structure whose morphology would correspond to the data reported earlier.[33-35] One of 2D AFM images used for 3D reconstruction (Figs. 4b, 4c) also indicates the absence of any distortions of the CLC planar structure in the vicinities of single QDs. Therefore, we may assume that, by using suitable surfactants, we may sufficiently increase the volume concentration of homogeneously distributed QDs without any considerable damage to the planar structure of the CLC matrix. According to our estimations, the average distance between individual QDs in our case is about 150 nm. Thus, it is likely that the volume concentration of such QDs can be increased by a factor of several tens.

3. CONCLUSION

We have developed a unique measurement technique for obtaining AFM, POM, fluorescence microspectroscopy, and SPN 3D nanostructure reconstructions for the same region of a sample. The main application of this technique is the study of exact relationship between the 3D morphology and optical properties of nanohybrid composites in which excitonic and plasmonic nanoparticles are embedded in polymer and liquid crystal matrices of different types.

We have used this technique to investigate the optical and morphological properties of a cholesteric LC matrix of a low-molecular-weight polymer doped with fluorescent CdSe/ZnS quantum dots. In previous studies, we showed that the fluorescence of QDs embedded in LCs was circularly polarized and that the dissymmetry factor of this polarization could be optically or electrically controlled via conformational changes in the helical structure of the LC matrix.[27,28] We also showed that such photo- and electro-active materials with a controlled degree of fluorescence circular polarization could be used for photochemical patterning or image recording, the recorded information being readable on the basis of changes in the dissymmetry factor of circular polarization of QD fluorescence.

The measurement technique developed in this study is a necessary tool for studying QD/CLC structures. We have demonstrated a correlation between POM images, spectral and morphological properties of the fluorescence of QDs embedded in the zones of the CLC matrix where QDs are homogeneously distributed and where they are aggregated into clusters. In the zone of homogeneous QD distribution, we have detected considerable modulation of the left-handed circularly polarized component of the QD fluorescence spectrum and a high negative fluorescence dissymmetry factor, whereas there was no modulation in the cluster zone. We have proposed a routine for quantitative estimation of the homogeneous solubility of single QDs in a CLC matrix, which is based on the data obtained by means of our complementary technique. Reconstruction of the 3D structure of the CLC matrix in the zone of homogeneous QD distribution has proved that single QDs embedded in the CLC matrix do not distort its periodic planar texture.

The results of this study and the measurement technique described here are potentially useful for nanotechnology, materials science, and biomedical research related to the development of different types of advanced nanohybrid materials with controlled optical properties, as well as for estimation of the effect of nanoparticles on biological materials. The new technique is expected to considerably facilitate the research and development of nanohybrid materials consisting of matrices of various types doped with semiconductor, metallic, carbon, and bioactive nanoparticles and nanoclusters. The types of the embedding matrices may widely vary: polymer and liquid crystal matrices, biomedical materials (pharmaceutical preparations and drug delivery systems), and biological objects (tissues, cells, and microorganisms).

4. MATERIALS AND METHODS

4.1 Chemicals

Cyclosiloxane (SilBlue**)** was purchased from Wacker Chemie (Munich, Germany). The chiral photochromic dopant 2,5-bis(4-methoxycinnamoyl)-1,4;3,6-dianhydro- D-sorbitol (Sorb) was synthesized as described in our previous study.[39]

4.2 Synthesis of quantum dots

CdSe/ZnS core/shell QDs were synthesized as described earlier.[40,41] Here, we used homogeneous QDs (size deviation, 10%) with CdSe cores approximately 5 nm in diameter (for QDs with emission at 604nm) with approximately 2 monolayers of the ZnS shell[42] and a quantum yield exceeding 60%. Synthesized QDs contained TOPO/TOP surfactants on their surface.[43] Photoluminescence of QDs was found to be stable during photopolymerisation and fluorescence excitation, with the variation of photoluminescence emission in the process of photopolymerisation not exceeding 10%.

4.3 Material and cell preparations

QD/CLC materials were prepared by dissolving SilBlue (96.3 wt%), Sorb (3.2 wt%), QDs with λ_{max} ~ 530 nm (0.05 wt%), and QDs with λ_{max} ~ 604nm (0.5 wt%) in chloroform and slow evaporating the solvent followed by drying the material in vacuum at 120°C. Aggregation and phase separation did not occur during the mixture preparation, and the mixtures prepared were homogeneous. The absence of relatively large aggregates of nanoparticles was confirmed by fluorescent and polarized optical microscopy. Note that dissolving of QDs did not lead to any noticeable changes in the optical quality of planar-oriented films, which remained transparent.

For optical and morphological studies, 20-μm films sandwiched between two flat glass plates were prepared. The thickness of the test samples was controlled with Teflon spacers. In order to obtain a good planar texture, we used the LC photo-alignment technique.[44] Glass plates were spin-coated with 2 mg/mL poly[1-[4-(3-carboxy-4-hydroxy-phenylazo) benzenesulfonamido]-1,2-ethanediyl, sodium salt (Sigma-Aldrich, St. Louis, MO, USA). After drying at room temperature, the glass plates coated with this polymer were irradiated with polarized polychromatic light by means of a mercury lamp (~15 mW/cm^2, 30 min). A Glan–Taylor prism was used as a polarizer.

The planar texture of QD/CLC was obtained by annealing the samples, which were heated to temperatures well above the glass transition temperature (140°C). After 30 min of annealing at the same temperature, two glass substrates were separated by shearing. As a result, two glass plates covered with a polymeric film were obtained. They were annealed for about another 30 min and then slowly cooled to room temperature at a rate of 1°C/min using a Mettler hot stage. After irradiation of the QD/CLC sample prior to the absorbance and fluorescence measurements, the samples were annealed for about 20 min and slowly cooled to room temperature at a rate of 1°C/min.

4.4 Study of phase behavior and optical and electro-optical analyses

The phase transition temperatures of the mixtures were determined using a LOMO P-112 polarizing optical microscope (St. Petersburg, Russia) equipped with a Mettler TA-400 hot stage (Mettler-Toledo, Greifensee, Switzerland). The transmittance spectra of planar-oriented films were recorded using a Unicam UV-500 UV-Vis spectrophotometer (Thermo Fisher Scientific, Waltham, MA, USA).

4.5 UMT/AFM/POM/fluorescence measurement

A step-by-step measurement scheme is presented on Figure 1.

Step I. Initial ultramicrotome sectioning of the LC films on a glass substrate was performed with the use of a Leica EM UC6NT ultramicrotome (Leica Microsystems GmbH, Austria). The area of the sectioned block face was no more than 1 mm^2 in order to simplify the location of the same area for complementary microscopic studies.

Step II. The POM images, fluorescence spectra, and 2D AFM images of the microtomed block face surface of the sample were obtained with the use of the combined AFM/POM/fluorescence spectroscopy setup. The sample sectioned as described above was placed directly on the top of the table for inverted optical microscopy with an open optical axis. The AFM head (SMENA, NT-MDT, Russia) was mounted onto the same optical table in the manner that allows the placement of the AFM probe tip within several micrometers from the optical axis. The spot of an LGN-519M Ar^+ laser (Plasma Ltd, Ryazan, Russia) used for sample irradiation was adjusted to the same spatial area through the deflectometer mirror of the AFM head as shown in Scheme S1. All optical images were obtained with an Optem Zoom 125C upright microscope adjusted to the overall optical axis passing through the same point as the AFM probe tip. The cross-polarized illumination system consisted of an ACE® Light Source, a homemade condenser lens system, a linearly polarizing polymer film (serving as a polarizer) placed directly on the condenser at an arbitrary or fixed angle, and a similar film (serving as an analyzer) placed into a rotatable CCD/microscope coupler. The fluorescence spectra were recorded using an M266 automated monochromator/spectrograph (SOLAR Laser Systems, Minsk, Belarus) with CCD U2C-16H7317 (Ormins, Minsk, Belarus) and a homemade light-collecting system with two Semrock 488-nm RazorEdge® ultrasteep long-pass edge filters (Rochester, NY, USA). The aforementioned Ar^+ laser operating at 488 nm was used for fluorescence excitation at a light intensity of 0.063 mW as measured by a LaserMate-Q (Coherent) intensity meter, with the beam focused into a spot with diameter a diameter of about 30 μm. The fluorescence spectra were recorded in an inverted mode with the use of a 20X/0.40 LCPlanFl lens (Olympus, Japan). 2D AFM images were obtained using the aforementioned AFM head; these images were used to locate the same area for SPN 3D reconstruction at the next step.

Step III. The area that had been analyzed by means of AFM/POM at the previous steps was located using optical microscopy and AFM, and the 3D structure of this area was reconstructed by the SPN technique. For SPN measurements and volume reconstruction, an NTEGRA-Tomo system (NT-MDT Co., Russia) was used, which comprised an AFM integrated with a Leica EM UC6NT ultramicrotome (Leica Microsystems GmbH, Austria) placed on a MOD-1 active vibration-protective table (Halcyonics GmbH, Germany).[37] The AFM measuring head in the "scanning by tip" configuration was mounted directly on the ultramicrotome knife holder over an Ultra AFM 35 diamond knife (Diatome AG, Switzerland). This construction allowed examining the sample surface with the AFM tip in a semicontact mode immediately after sectioning, when the ultramicrotome arm was in the highest position. The cantilever tips used for AFM measurements were NSC15 (Micromash, Estonia) with a characteristic resonant frequency of about 325 kHz; the radius was below 10 nm. The 3D reconstruction was obtained by means of sample surface imaging alternated with serial ultramicrotoming. The minimum section thickness used in the present study was 50 nm. The ImagePro Plus 6.0 post-processing software (Media Cybernetics, Inc.) with a 3DConstructor option for the automated image alignment and visualization of 3D images was used for spatial reconstruction.

For 3D reconstruction of the periodic structure of the CLC matrix doped with QDs, a QD–CLC mixture was deposited on a PTFT substrate, embedded in epoxy resin, and ultramicrotomed in the plane parallel to the helix axis. Then, a series of ultramicrotome sections with the same section thickness, each followed by AFM measurements, were performed.

ACKNOWLEDGMENTS

This study was partly supported by the Ministry of Higher Education and Science of the Russian Federation (grant nos. 1.G34.31.0050 and Contract no. 8842), the European Commission through the FP7 Cooperation Program (grant no. NMP-2009-4.0-3-246479 NAMDIATREAM). and the Russian Foundation for Basic Research (grant nos. 13-04-00168, 11-03-01046, 12-03-00553-a and 11-02-00369-a). I.N. acknowledges the programs HYNNOV and Nano'Mat supported by the Champagne-Ardenne region, the DRRT Champagne-Ardenne and the FEDER. We thank Vladimir Ushakov for the help in the preparation of the manuscript.

REFERENCES

[1] Möbus, G. and Inkson, B.J., "Nanoscale tomography in materials science," Materials Today 10(12), 18-25 (2007).

[2] Midgley, P. A. and Dunin-Borkowski, R. E., "Electron tomography and holography in materials science," Nature Mater. 8, 271-280 (2009).

[3] Bavel, S. and van Loos, J., "Volume Organization of Polymer and Hybrid Solar Cells as Revealed by Electron Tomography, " Adv. Funct. Mater. 20, 3217 (2010).

[4] Medalia, O., Weber, I., Frangakis, A.S., Nicastro, D., Gerisch, G. and Baumeister, W., "Macromolecular architecture in eukaryotic cells visualized by cryoelectron tomography," Science 298, 1209–1213 (2002).

[5] Milne, J. and Subramaniam, S., "Cryo-electron tomography of bacteria: progress, challenges and future prospects, " Nature Reviews Microbiology 7, 666-675 (2009).

[6] Holzer, L., Indutnyi, F., Gasser, P., Munch B. and Wegmann, M., "Three-dimensional analysis of porous BaTiO3 ceramics using FIB nanotomography," J. Microsc. 216, 84 (2004).

[7] Al-Abboodi, A., Fu, J., Doran, P. M. and Chan, P. P. Y., "Three-Dimensional Nanocharacterization of Porous Hydrogel With Ion and Electron Beams," Biotechnol. Bioeng. 110(1), 318-326 (2013).

[8] Weston, A. E., Armer, H. E. J. and Collinson, L. M., "Towards native-state imaging in biological context in the electron microscope," J. Chem. Biol. 3(3), 101-112 (2010).

[9] Rossmann, M. G., Battisti, A. J. and Plevka P., "Future prospects," Adv. Protein Chem. Struct. Biol. 82, 101-121 (2011).

[10] Binnig, G., Gerber, C., Stoll, E., Albrecht, T.R. and Quate, C.F., "Atomic resolution with atomic force microscope," Eur. Lett. 3, 1281-1286 (1987).

[11] Magonov, S. N. and Reneker, D.H., "Characterization of polymer surfaces with atomic force microscopy," Annu. Rev. Mater. Sci. 27, 175-222 (1997).

[12] Efimov, A. E., Tonevitsky, A. G., Dittrich, M. and Matsko, N. B., "Atomic force microscope (AFM) combined with the ultramicrotome: a novel device for the serial section tomography and AFM/TEM complementary structural analysis of biological and polymer samples," Journal of Microscopy 226(3), 207–217 (2007).

[13] Efimov, A. E., Gnaegi, H., Schaller, R., Grogger, W., Hofer, F. and Matsko, N. B., "Analysis of native structure of soft materials by cryo scanning probe tomography," Soft Matter 8, 9756-9760 (2012).

[14] Alekseev, A., Efimov, A., Lu, K. and Loos, J., "Three-dimensional electrical property reconstruction of conductive nanocomposites with nanometer resolution," Advanced Materials 21(48), 4915 – 4919 (2009).

[15] Alekseev, A., Chen, D., Tkalya, E. E., Ghislandi, M. G., Syurik, Yu., Ageev, O., Loos, J. and De With, G., "Local organization of graphene network inside graphene/polymer composites," Adv. Funct. Mater. 22(6), 1311-1318 (2012).

[16] Matsko, N. B., "Atomic force microscopy applied to study macromolecular content of embedded biological material," Ultramicroscopy 107, 95–105 (2007).

[17] Matsko, N. B. and Mueller, M., "AFM of biological material embedded in epoxy resin," J. Struc. Biol. 146, 334-343 (2004).

[18] Mirzaei, J., Reznikov, M., and Hegmann, T., "Quantum dots as liquid crystal dopants," J. Mater. Chem. 22(42), 22311–22798 (2012).

[19] Stamatoiu, O., Mirzaei, J., Feng X. and Hegmann, T., "Nanoparticles in liquid crystals and liquid crystalline nanoparticles," Top. Curr. Chem. 318, 331–393 (2012).

[20] Shivakumar, U., Mirzaei, J., Feng, X., Sharma, A.., Moreira, P. and Hegmann, T., "Nanoparticles – versatile, promising yet challenging dopants for liquid crystals," Liq. Cryst. 38, 1495–1514 (2011).

[21] Hegmann, T., Qi, H. and Marx, V. M, "Nanoparticles and liquid crystals: synthesis, self-assembly, defect formation and potential applications,"J. Inorg. Organomet. Polym. & Mater. 17, 483–508 (2007).

[22] Qi, H. and Hegmann, T., "Impact of nanoscale particles and carbon nanotubes on current and future generations of liquid crystal displays," J. Mater. Chem. 18, 3288–3294 (2008).

[23] Lagerwall, J. P. F. and Scalia, G., "A new era for liquid crystal research: Applications of liquid crystals in soft matter nano-, bio- and microtechnology," Curr. Appl. Phys. 12(6), 1387–1412 (2012).

[24] Bisoyi, H. K. and Kumar, S., "Liquid crystal nanoscience: an emerging avenue of soft self-assembly," Chem. Soc. Rev. 40, 306–319 (2011).

[25] Blinov, L.M. and Chigrinov, V.G., [Electrooptic Effects in Liquid Crystal Materials], Springer Verlag, New York, (1993).
[26] Tong, X. and Zhao, Y., "Liquid-crystal gel-dispersed quantum dots: reversible modulation of photoluminescence intensity using an electric field," J. Am. Chem. Soc. 129, 6372–6373 (2007).
[27] Bobrovsky, A., Mochalov, K., Oleinikov, V., Shibaev, V., "Glass-forming photoactive cholesteric oligomers doped with quantum dots: novel materials with phototunable circularly polarised emission," Liq. Cryst. 38(6), 737-742 (2011).
[28] Bobrovsky, A., Mochalov, K., Oleinikov, V., Sukhanova, A., Prudnikau, A., Artemyev, M., Shibaev, V. and Nabiev, I., "Optically and electrically controlled circularly polarized emission from cholesteric liquid crystal materials doped with semiconductor quantum dots," Adv. Mater. 24, 6216–6222 (2012).
[29] Lukishova, S. G., Bissell, L. J., Winkler J. and Stroud, C. R., "Resonance in quantum dot fluorescence in a photonic bandgap liquid crystal host,"Opt. Lett. 37(7), 1259–1261 (2012).
[30] Lukishova, S. G., Bissell, L. J., Stroud, Jr. C. R. and Boyd, R.W., "Room-temperature single photon sources with definite circular and linear polarizations," Optics and Spectroscopy 108 (3), 417-424 (2010).
[31] Grangier, P., Sanders, B. and Vuckovic, J., "Focus on single photons on demand," New J. Phys. 6, (2004).
[32] Kopp, V. I., Fan, B., Vithana, H. K. M. and Genack, A. Z., "Low-threshold lasing at the edge of a photonic stop band in cholesteric liquid crystals," Optics Lett. 23(21), 1707-1709 (1998).
[33] Meister, R., Halle´, M.-A., Dumoulin, H. and Pieranski, "Structure of the cholesteric focal conic domains at the free surface," P. Phys. Rew. E 54(4) (1996).
[34] 35Boudet, A., Mitov, M., Bourgerette, C., Ondarcuhu, T. and Coratger, R., "Glassy cholesteric structure: thickness variation induced by electron radiation in transmission electron microscopy investigated by atomic force microscopy," Ultramicroscopy 88(4), 219–229, (2001).
[35] Agez, G., Bitar R. and Mitov M., "Color selectivity lent to a cholesteric liquid crystal by monitoring interface-induced deformations," Soft Matter 7, 2841–2847 (2011).
[36] Dintinger, J., Tang, B.-J., Zeng, X., Kienzler, T., Mehl, G. H., Ungar, G., Rockstuhl C. and Scharf, T., "Optical properties of mesogen-coated gold nanoparticles," Proc. of SPIE 8271, 061-066 (2012).
[37] Milette, J., Cowling, S. J., Toader, V., Lavigne, C., Saez, I. M., Lennox, R. B., Goodby, J. W. and Reven, L. "Reversible long-range patterning of gold nanoparticles by smectic liquid crystals," Soft Matter 8, 2593-2598 (2012).
[38] Rozic, B., Karatairi, E., Nounesis, G., Tzitzios, V., Cordoyiannis, G., Kralj, S. and Kutnjak, Z., "Impact of surface-functionalized CdSe nanoparticles on phase transitions of 8CB and CE8 liquid crystals," Mol. Cryst. Liq. Cryst., 553, 161–167 (2012).
[39] Bobrovsky, A., Boiko, N. and Shibaev, V., "New chiral-photochromic dopant with variable helical twisting power and its use in photosensitive cholesteric materials," Mol. Cryst. Liq. Cryst., 363, 35-50, (2001).
[40] Sukhanova, A., Venteo, L., Devy, J., Artemyev, M., Oleinikov, V., Pluot, M. and Nabiev, I., "Highly stable fluorescent nanocrystals as a novel class of labels for immunohistochemical analysis of paraffin-embedded tissue sections," Lab. Invest. 82, 1259–1261 (2002).
[41] Sukhanova, A., Devy, J., Venteo, L., Kaplan, H., Artemyev, M., Oleinikov, V., Klinov, D., Pluot, M., Cohen J.H.M. and Nabiev, I., "Biocompatible fluorescent nanocrystals for immunolabeling of membrane proteins and cells," Anal Biochem. 324(1), 60-67 (2004).
[42] Baranov, A.V., Rakovich, Yu.P., Donegan, J.F., Perova, T.S., Moore, R.A., Talapin, D. V., Rogach, A.L., Masumoto, Y. and Nabiev, I., "Effect of ZnS shell thickness on the phonon spectra in CdSe quantum dots," Phys. Rev. B 68, 165306-1 (2003).
[43] Wargnier, R., Baranov, A., Maslov, V., Stsiapura, V., Artemyev, M., Pluot, M., Sukhanova, A. and Nabiev, I., "Energy transfer in aqueous solutions of oppositely charged CdSe/ZnS core/shell quantum dots and in quantum dot-nanogold assemblies," Nano Lett. 4(3), 451-457 (2004).
[44] Bobrovsky, A., Ryabchun, A., Shibaev, V., "Liquid crystals photoalignment by films of side-chain azobenzene-containing polymer with different molecular structure," J. Photochem. Photobiol., A: Chemistry 218, 137-142 (2011).